Three-Dimensional CFD Model of the Deaeration Rate of FCC Particles

Sanjib Das Sharma and Todd Pugsley
Dept. of Chemical Engineering, University of Saskatchewan, Saskatoon, Saskatchewan S7N 5A9, Canada

Romain Delatour
Total Research Centre, Lyon, France

DOI 10.1002/aic.10858
Published online April 6, 2006 in Wiley InterScience (www.interscience.wiley.com).

Computational fluid dynamics (CFD) has been used to model the deaeration rate for a fluidized bed of fluid catalytic cracking (FCC) catalyst. The Eulerian approach has been used in which the gas and solid phases present in the fluidized bed are treated as interpenetrating continua with constitutive equations obtained from the granular kinetic theory and the interphase drag relationship. Using the CFD code MFIX, transient calculations have been made for a three-dimensional (3-D) cylindrical vessel of 0.104 m diameter. Various cases have been modeled: fluidization at superficial gas velocities of 0.005 and 0.028 m/s followed by deaeration for two catalyst bed masses of 3.17 and 4.05 kg. These have been performed for monosize particles of Sauter mean diameters of 69.8 and 100 microns. The results have been presented in terms of variation of gauge pressure with time at a height of 30 cm above the distributor plate. Comparisons of these predictions with the experimental data show that the deviation between the experimental results and the CFD predictions of deaeration rate is <10%. Based on these results it appears that our CFD modeling approach, which includes the introduction of an empirical correction factor for the gas–solid drag term, can adequately predict the deaeration rate of FCC catalyst using a single mean particle size. © 2006 American Institute of Chemical Engineers *AIChE J,* 52: 2391–2400, 2006

Keywords: CFD, deaeration, fluidization, FCC, modeling

Introduction

Flowability of fluid catalytic cracking (FCC) catalyst in vertical and angled standpipes and U-bends is important for maintaining stable circulation in fluid catalytic cracking units (FCCUs). To maintain stable circulation, the catalyst should be in a fluidized state. Deaeration of catalyst in the standpipe will lead to defluidization and thus catalyst circulation problems. The deaeration test may be used to quantify the tendency of different catalysts to deaerate.

There are two main types of catalyst deaeration tests. The first, which is known as the bed collapse test, involves suddenly cutting off the air supply to a fluidized bed containing the catalyst and plotting the height of the upper bed level vs. time. The deaeration rate is then calculated based on the time it takes for the bed to return to its nonexpanded level. The second type of deaeration test measures the time after the air supply is cut off for the dense–dilute interface to cross a pressure probe positioned at a given distance above the distributor. The deaeration rate is calculated by dividing the distance above the distributor by the time. One manifestation of this is the Engelhard test, which is discussed later in the experimental section of this article.

There are several experimental studies involving the collapse

Correspondence concerning this article should be addressed to T. Pugsley at Todd.Pugsley@usask.ca.

test that have been published in the open literature. The test has been used by researchers to determine the average voidage of the dense phase in bubbling beds of Group A powders.[1-5] Some researchers have assumed that the deaeration rate is equal to the superficial gas velocity in the dense phase of the bubbling bed.[6,7] The bed collapse test has also been used as a quantitative test to characterize the fluidization quality of different classes of powders[8,9] and to investigate the effect of fines on the fluidization of fine catalyst powders.[10]

In addition to yielding valuable experimental results related to powder characterization and fluidized bed hydrodynamics, the deaeration test bed is an excellent system to model with computational fluid dynamics (CFD). Although the experiment is simple, various important features of gas–solid fluidization such as bed expansion, bubbling, sedimentation, and consolidation all play important roles during the bed collapse. Furthermore, the test is done at small scale, which allows the full three-dimensional geometry to be defined in the CFD model while maintaining reasonable computational times to achieve a stable converged solution. This capacity to model a fluidized bed using CFD in three dimensions is important; Peirano et al.[11] reported differences in the predictions of power spectral density and expanded bed height obtained from 2-D and 3-D CFD models of a fluidized bed containing silica sand. McKeen and Pugsley[12] reported even greater variations in predicted bed expansion between 2-D and 3-D CFD models for fluidized beds containing FCC catalyst powder. Given that the deaeration test for FCC catalyst begins from an expanded state, it is important to be able to accurately model bed expansion.

The only previous CFD modeling study of the fluidized bed collapse test is that of Gelderbloom et al.[13] There appears to be no CFD modeling studies of the Englehard test or similar deaeration tests based on the detection of the dense–dilute interface as it reaches a pressure probe immersed in the bed. Gelderbloom et al.[13] compared their model predictions with data for bed collapse velocity and found favorable agreement. They also found that the general shape of their plots of bed height as a function of time during bed collapse followed the experimental trends reported by other authors. However, a closer look at their plots reveals the same unrealistic bed expansion reported by McKeen and Pugsley.[12] The expanded bed heights in the plots of Gelderbloom et al.[13] at the time when the fluidizing gas is shut off are 75 to 80% greater than the final consolidated bed heights. This is explained by the use of the default drag relationships in multiphase flow with interphase exchanges (MFIX); as will be discussed later, McKeen and Pugsley[12] found that these relationships require modification to overcome the unrealistic predictions of bed expansion. Gelderbloom et al.[13] also found that the solid-phase modulus, which takes into account the variation of the solid pressure with the solid volume fraction, is the controlling parameter in the consolidation regime. Furthermore, based on their CFD model predictions, they concluded that the traditional interpretation of the collapsing bed as consisting of separate bubble escape and sedimentation regimes is incorrect and that in fact these phenomena occur simultaneously.

Given that the study of Gelderbloom et al.[13] looked only at bed collapse and that their results overestimate bed expansion, further CFD modeling work is warranted. In the present work, a three-dimensional, transient CFD study is carried out to simulate the deaeration test for FCC catalyst (Geldart A powder). The CFD code MFIX (www.mfix.org), available from the U.S. Department of Energy's National Energy Technology Laboratory (NETL), has been used to solve the system of partial differential equations and closure relations. The CFD model predictions are presented in terms of the variation of gauge pressure with time at a height of 30 cm above the distributor and are validated by comparison with experimental deaeration test data.

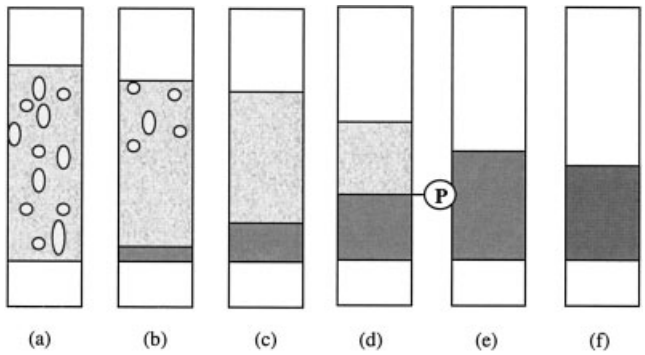

Figure 1. Progress of a typical fluidized bed deaeration experiment.

Experimental

The so-called Englehard test[14] measures the time for the pressure measured 30 cm (1 ft) above the distributor to return to zero once the fluidizing air to the test bed has been shut off. A limitation of this test is that, by the time the pressure reading reaches zero, the portion of the bed below the pressure probe has been completely defluidized for some time (that is, the air velocity in the lower part of the bed is below the minimum value required for fluidization). Thus this is not a particularly good indicator of the capacity of the catalyst to stay in the fluidized state. Furthermore, with respect to catalyst circulation in a FCCU, it is the difference between minimum fluidization and minimum bubbling velocities of a catalyst that is important for defining the stable operating range in the standpipe. The Englehard test provides no indication of this difference.

The Englehard test may be improved on by looking more closely at the pressure vs. time curve after the fluidizing air is stopped. The progress of a typical deaeration experiment and the corresponding variation of pressure at a particular height in the bed as a function of time are shown in Figures 1 and 2. After the air supply is stopped, the bubbles rise rapidly through the bed (Figures 1a and 1b). The release of all the bubbles from the bed is marked by a change in the slope of the pressure vs. time plot (point b in Figure 2). The air continues to exit the bed, forming a dense zone at the bottom of the bed (Figure 1b) with an incipiently fluidized bed above. The dense–dilute interface moves upward with time (Figures 1c and 1d) and the pressure at the measurement point gradually decreases along the curve denoted as "c " in Figure 2. This decrease in pressure reflects the reduction in the mass of solids above the measurement point as the bed settles. When the dense–dilute interface reaches the pressure measurement point P (Figure 1d), a sharp change in the slope of the pressure plot takes place (point d in Figure 2). From this point onward, the pressure decreases more rapidly as the dense–dilute interface continues to rise until all

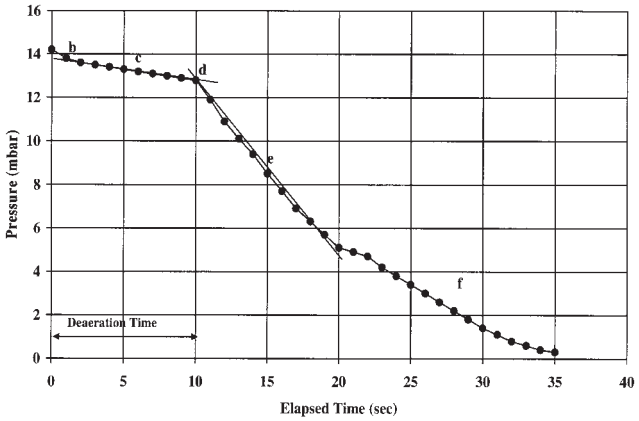

Figure 2 Variation of gauge pressure with time at a particular axial position above

Figure 2. Variation of gauge pressure with time at a particular axial position above the distributor plate.

of the particles have settled and all of the entrapped air has escaped from the bed (Figures 1e and 1f). The dense–dilute interface represents the interface between a defluidized zone and a fluidized bed. The time it takes for this interface to reach the measurement point may be used to calculate the deaeration rate, as indicated in Figure 2. This method of determining the deaeration rate is an improvement on the Englehard test because it focuses only on the time it takes for the dense–dilute interface to pass the measurement point. This is a better indication of the deaeration rate as it applies to standpipe flow because beyond that time in the pressure–time curve, the portion of the bed below the measurement point is defluidized. Operation of a standpipe in a defluidized state is not conducive to optimal catalyst circulation in the FCCU.

The improved deaeration test has been used to collect deaeration rate data for model validation in the present study. The data were collected at the Total Research Centre in the 10.5-cm ID cylindrical test bed schematically illustrated in Figure 3. A stainless steel pressure probe was inserted into the bed to a depth of 30 cm above the distributor plate. The pressure probe was connected to a pressure transducer and a computerized data acquisition system to collect pressure vs. time data at this depth.

The experimental conditions as well as the FCC catalyst physical properties are summarized in Table 1. Two superficial gas velocities and two mean particle sizes were tested as well as two catalyst bed masses. Details of the particle size distribution have been omitted for proprietary reasons, although the differences in the mean sizes of the catalyst reflect different percentages of fines < 44 microns in the two experiments. The influence of fines content on the fluidized nature of catalyst powders has been documented in several studies.[8,10,15-17] A certain fraction of fines in a mixture of FCC catalyst is also considered to be important for smooth catalyst circulation in most FCCUs because the addition of fines increases the ratio of minimum bubbling to minimum fluidization velocity. Thus it should be expected that the presence of fines will influence the deaeration test.

Governing Equations

The CFD model used in this work is based on the extended two-fluid model (TFM), which uses granular kinetic theory for

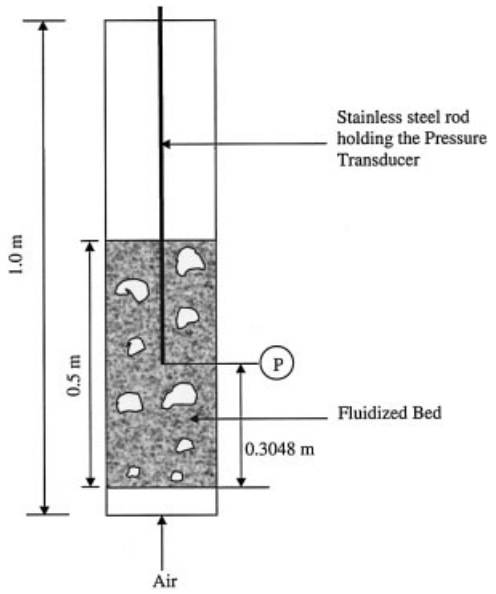

Figure 3. Deaeration test bed.

the particulate phase. Particles are considered to be smooth, spherical, inelastic, and to undergo binary collisions. The fundamental equations of mass, momentum, and energy conservation are solved for each phase. Appropriate constitutive equations are specified to describe the physical and rheological properties of each phase and to close the conservation equations. The granular temperature is estimated by solving a fluctuating kinetic energy equation for the particles. The solid viscosity and the pressure can then be computed as a function of the granular temperature at any time and position. The conservation equations are written as follows.

Volume fraction

$$\varepsilon_g + \varepsilon_s = 1 \tag{1}$$

Gas-phase continuity

$$\frac{\partial}{\partial t}(\varepsilon_g \rho_g) + \nabla \cdot (\varepsilon_g \rho_g \vec{v}_g) = 0 \tag{2}$$

Solids-phase continuity

$$\frac{\partial}{\partial t}(\varepsilon_s \rho_s) + \nabla \cdot (\varepsilon_s \rho_s \vec{v}_s) = 0 \tag{3}$$

Table 1. Experimental Conditions and Catalyst Physical Properties

Inlet gas velocity	0.005 m/s, 0.028 m/s
Average particle size	69.8 μm, 100 μm
Particle density	1310 kg/m^3
Bulk density	850 kg/m^3
U_{mf}	0.0017 m/s
U_{mb}	0.006 m/s
ε_{mf}	0.4
ε_{mb}	0.49
Catalyst mass	3.17 kg, 4.05 kg

Gas-phase momentum

$$\frac{\partial}{\partial t}(\varepsilon_g \rho_g \vec{v}_g) + \nabla \cdot (\varepsilon_g \rho_g \vec{v}_g \vec{v}_g) = -\varepsilon_g \nabla P_g + \nabla \cdot \bar{\bar{\tau}}_g + F_{gs}(\vec{v}_s - \vec{v}_g) + \varepsilon_g \rho_g \vec{g} \quad (4)$$

Solids-phase momentum

$$\frac{\partial}{\partial t}(\varepsilon_s \rho_s \vec{v}_s) + \nabla \cdot (\varepsilon_s \rho_s \vec{v}_s \vec{v}_s) = -\varepsilon_s \nabla P_g + \nabla \cdot \bar{\bar{S}}_s - F_{gs}(\vec{v}_s - \vec{v}_g) + \varepsilon_s \rho_s \vec{g} \quad (5)$$

For the continuity equations the first term accounts for the rate of mass accumulation per unit volume and the second term represents the net convective flux of mass. In the momentum equations, the first term on the left represents the net rate of change of momentum, whereas the second term on the left accounts for the net rate of momentum transfer by convection. On the right-hand side, the first term represents buoyancy force, the second term accounts for stresses arising from normal and shear forces, the third term is momentum transfer resulting from gas–solids drag, and finally the fourth term accounts for the body force arising from gravity.

Closure Relations

Closure relations for the gas-phase stress $\bar{\bar{\tau}}_g$, granular stress $\bar{\bar{S}}_s$, and gas–solids drag F_{gs} are needed to solve the above set of equations. The only interaction forces considered between the two phases are drag and buoyancy; the particle–particle collision forces are grouped into the granular stress term.

Gas–solids drag

Previous work from our group[12,18] as well as the work of van Wachem et al.[19] illustrated how the existing published drag laws give very similar predictions of the drag force for a given voidage and relative velocity. However, these drag laws, when incorporated into CFD models of bubbling beds of FCC catalyst, lead to overpredictions of bed expansion and correspondingly unrealistic voidages.[12,20] The main limitation with all of the available gas–solid drag laws in the context of the present study is that they were all developed by fitting data for particles much larger than the Geldart A particles considered here. Furthermore, gas–solid drag laws are all based on data corresponding to uniform voidage (packed bed, uniformly expanded bed, or sedimentation), and thus apply to CFD only when the voidage within a computational cell is uniform. In the case of the formation of particle clusters smaller than a computational cell, the standard gas–solids drag correlations are no longer valid.

In the present work, we have followed the approach of McKeen and Pugsley[12] whereby the drag law of Gibilaro et al.[21] is modified by using a fractional scale factor denoted as C to reduce the drag force:

$$F_{gs} = C\left(\frac{17.3}{\mathrm{Re}_p} + 0.336\right)\frac{\rho_g|\vec{v}_s - \vec{v}_g|}{d_p}\varepsilon_s \varepsilon_g^{-1.8} \quad (6)$$

where

$$\mathrm{Re}_p = \frac{\rho_g d_p |\vec{v}_s - \vec{v}_g| \varepsilon_g}{\mu_g} \quad (7)$$

Recent work by Ye[22] also reported the use of the correction factor for the drag force when modeling bubbling beds of fine powder. The theoretical basis of this correction factor is presented in the Appendix and follows the approach that has been used to include cohesive forces in distinct element method (DEM) simulations.[23,24]

Our previous modeling effort was for a freely bubbling bed of FCC catalyst where a correction factor C, in the range of 0.2 to 0.3, was used.[12] The present study involves not only the modeling of a bubbling bed, but also an expanded bed in which bubbles are absent. Thus we had to consider how to incorporate the drag correction factor C. The sensitivity of the model predictions to the value of the correction factor was tested and it was found that, consistent with the work of McKeen and Pugsley,[12] to obtain predictions that agreed with the experimental bed expansion data, a value of $C = 0.25$ was needed for the 0.028 m/s case. For the lower velocity case (0.005 m/s) in the present study, the bed was operating between the minimum fluidization and minimum bubbling velocities, as it is during the deaeration step, after the initial rapid loss of bubbles. In this case, a value of $C = 1$ (that is, no correction to the Gibilaro et al.[21] model) was needed when no bubbles were present in the bed. For the deaeration step, again the value of C was set equal to 1; otherwise, unrealistically high deaeration rates were predicted. The fact that no correction factor is needed when there are no bubbles in the bed is consistent with the fact that the published interphase drag relationships were developed for liquid–solid systems. A bed of FCC catalyst behaves like a liquid–solid system when it is operated in the stable expanded state between minimum bubbling and minimum fluidization conditions.

Gas-phase stress

The standard Newtonian form is assumed for the gas-phase stress:

$$\bar{\bar{\tau}}_g = 2\mu_g \bar{\bar{D}}_g - \frac{2}{3}\mu_g tr(\bar{\bar{D}}_g)\bar{\bar{I}} \quad (8)$$

In this study, gas-phase turbulence is not considered because it is assumed to be dampened by the presence of the particles in the dense bed.[19]

Granular stress

Granular flows can be classified into two distinct flow regimes: (1) a plastic regime, arising from frictional forces between particles in dense flow; and (2) a viscous regime, arising from collisional transport of momentum. The solids-phase stress tensor is given by the following equation:

$$\bar{\bar{S}}_s = \begin{cases} -P_s^p \bar{\bar{I}} + \bar{\bar{\tau}}_s^p & \text{if } \varepsilon_g \le \varepsilon_g^* \\ -P_s^v \bar{\bar{I}} + \bar{\bar{\tau}}_s^v & \text{if } \varepsilon_g > \varepsilon_g^* \end{cases} \quad (9)$$

The superscript p denotes the plastic regime and the superscript v denotes the viscous regime. The critical packing ε_g^* is normally set at the minimum fluidization voidage for fluidized bed simulations.

In the plastic regime, the solids pressure is defined by a relation that allows a certain amount of compressibility in the solids phase:

$$P_s^p = 10^{25}(\varepsilon_s - \varepsilon_s^{cp})^{10} \tag{10}$$

For most simulations, $\varepsilon_s^{cp} = \varepsilon_g^*$, meaning that the particles form a close-packed arrangement at the specified critical packing ε_g^*. The solids stress tensor is calculated by a relation from Schaeffer[25]:

$$\bar{\bar{\tau}}_s^p = 2\mu_s^p \bar{\bar{D}}_s \tag{11}$$

where

$$\mu_s^p = \frac{P_s^p \sin\phi}{2\sqrt{I_{2Ds}}} \tag{12}$$

$$I_{2Ds} = \frac{1}{6}\left[(D_{s11} - D_{s22})^2 + (D_{s22} - D_{s33})^2 + (D_{s33} - D_{s11})^2\right] + D_{s12}^2 + D_{s23}^2 + D_{s31}^2 \tag{13}$$

$$\bar{\bar{D}}_s = \frac{1}{2}\left[\nabla\vec{v}_s + (\nabla\vec{v}_s)^T\right] \tag{14}$$

Inclusion of the plastic flow regime models gives a better representation of the movement of packed regions in a fluidized bed.

In the viscous regime, the equations for pressure and stress were developed by Lun et al.[26] from a theory similar to the kinetic theory of dense gases by considering random interparticle inelastic collisions. The equations are as follows:

$$P_s^v = K_1 \varepsilon_s^2 \Theta \tag{15}$$

$$\bar{\bar{\tau}}_s^v = \lambda_s^v tr(\bar{\bar{D}}_s)\bar{\bar{I}} + 2\mu_s^v \bar{\bar{D}}_s \tag{16}$$

where the second coefficient of viscosity is

$$\lambda_s^v = K_2 \varepsilon_s \sqrt{\Theta} \tag{17}$$

and the shear viscosity is

$$\mu_s^v = K_3 \varepsilon_s \sqrt{\Theta} \tag{18}$$

The remaining constants are defined as

$$K_1 = 2(1+e)\rho_s g_0 \tag{19}$$

$$K_2 = \frac{4 d_p \rho_s (1+e)\varepsilon_s g_0}{3\sqrt{\pi}} - \frac{2}{3}K_3 \tag{20}$$

$$K_3 = \frac{d_p \rho_s}{2}\left\{\frac{\sqrt{\pi}}{3(3-e)}\left[1 + 0.4(1+e)(3e-1)\varepsilon_s g_0\right] + \frac{8\varepsilon_s g_0 (1+e)}{5\sqrt{\pi}}\right\} \tag{21}$$

$$K_4 = \frac{12(1-e^2)\rho_s g_0}{d_p\sqrt{\pi}} \tag{22}$$

The radial distribution function at contact, g_0, accounts for the increase in probability of collisions as the particle concentration is increased. In this work, we have used the g_0 formulation of the Carnahan and Starling model:

$$g_0 = \frac{1}{\varepsilon_g} + \frac{3\varepsilon_s}{2\varepsilon_g^2} \tag{23}$$

Assuming granular energy is dissipated locally, neglecting convection and diffusion terms, and retaining only generation and dissipation terms:

$$(-P_s^* I + \tau_s) \quad : \quad \nabla\vec{v}_s - \gamma = 0 \tag{24}$$

Such an assumption is valid only for very dense gas–solid systems like the bubbling bed.[27]

The above equation can be solved for Θ to obtain the following equation:

$$\Theta = \left\{\frac{-K_1\varepsilon_s tr(\bar{\bar{D}}_g) + \sqrt{K_1^2 tr^2(\bar{\bar{D}}_s)\varepsilon_s^2 + 4K_4\varepsilon_s[K_2 tr^2(\bar{\bar{D}}_s) + 2K_3 tr(\bar{\bar{D}}_s^2)]}}{2\varepsilon_s K_4}\right\}^2 \tag{25}$$

Model Geometry, Initial and Boundary Conditions, and Numerical Parameters

All simulations were run using a distributed-memory parallel version of MFIX on the Bioinformatics and Computational Biology Research Laboratory (BIRL) Beowulf computer cluster at the University of Saskatchewan. The three-dimensional model geometry defined in MFIX was based on the dimensions of the test bed at the Total Research Centre (Figure 3). Figure 4 illustrates the geometry for the catalyst mass of 3.17 kg, including the initial and boundary conditions. It is important to point out that, although the vessel used by Total for deaeration tests was 1 m tall, a 0.70 m tall vessel has been modeled here for the catalyst mass of 3.17 kg. This reflects the need for very small time steps and small grid size when modeling beds containing a fine catalyst and the large number of nodes when carrying out a three-dimensional simulation, even for a relatively small vessel such as this one. In an effort to reduce computation time, the height of the vessel in our model was made less than that of the actual test vessel. We feel that the reduction in height of the test vessel will not adversely affect our results because the expanded height of the test bed is well below 0.7 m. The static bed height of 0.5 m shown in Figure 4 was determined from the weight of the catalyst used in the Total tests and the voidage of the bed at minimum fluidization.

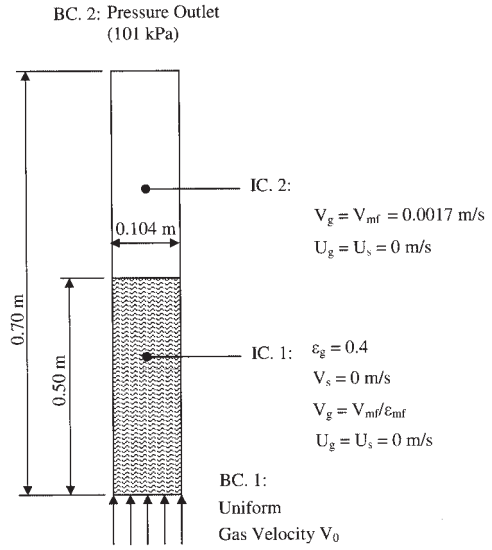

Figure 4. Typical test bed geometry used in the CFD model for the 3.17 kg bed mass, showing initial and boundary conditions.

With similar logic, a column height of 0.85 m and a minimum fluidized bed height of 0.61 m were used for the catalyst mass of 4.05 kg.

A uniform cell size of 0.005 m has been used in the simulations for the inlet gas velocity of 0.005 m/s. This cell size was reported to be sufficiently small for obtaining a numerical solution that is grid independent.[12] For the higher inlet gas velocity of 0.028 m/s, cell sizes of 0.001, 0.003, and 0.005 m were used to test the grid dependency of the solution in terms of resolution of bubble shape and time of computation. Of these, the 0.005 m cell size resulted in the poorest resolution of bubbles but the least computation time (15 s of real time computation completed in 2 weeks), whereas a cell size of 0.001 m resulted in much improved bubble resolution, but substantially increased the computation time (only 3 s of real time computation completed in 2 weeks) because of the increase in the total number of grid cells. The simulations were also more unstable with frequent divergence, thereby requiring a very small time step (about 0.00005–0.0001 s). With the 0.003 m cell size, a compromise between these two was obtained with a better bubble resolution than the 0.005 m grid cell but lesser computation time than the 0.001 m cell size (about 10 s of real time computation completed in 2 weeks). Thus, a uniform cell size of 0.003 m was used for the higher velocity case.

The inlet gas was air at 27°C and was evenly distributed over the bottom of the bed. The outlet boundary condition was a specified constant pressure (atmospheric); solids are free to leave if entrained, and are not returned to the computational domain. At the walls, the no-slip condition was applied for the gas phase. For the solid phase, the partial slip condition was used for the solids velocity by using the Johnson–Jackson boundary condition[28]:

$$V_{s,w} = -A \frac{\partial V_{s,w}}{\partial n} \tag{26}$$

where

$$A = \frac{6\mu_s \varepsilon_{s,\max}}{\sqrt{3}\,\pi\varphi\rho_s\varepsilon_s g_0 \sqrt{\Theta_s}} \tag{27}$$

and φ is the specularity coefficient. In all our simulations we have considered $\varphi = 0.005$.

The bed was assumed to be at the minimum fluidization condition initially, which corresponded to a solid volume fraction of 0.6 (that is, ε_{mf} of 0.4). The solid velocity was initially set to zero, whereas the gas velocity inside the bed was set to the interstitial gas velocity at minimum fluidization conditions. From the upper bed surface to the exit of the test vessel, the gas velocity was set equal to the minimum fluidization velocity.

Table 2 summarizes the numerical parameters for the simulations. The restitution coefficient for particle–particle collisions is based on Benyahia et al.[29] for FCC particles. Previous work by our group has found that CFD predictions of bubbling fluidized beds are insensitive to changes in this parameter.[18] The angle of internal friction, used for calculating granular stress in the frictional flow regime, is typical for FCC powders. The voidage at maximum packing had to be set near the

Table 2. Simulation Parameters Used in MFIX

Geometry	Three-dimensional, cylindrical
Height of test vessel	0.7 m, 0.85 m
Diameter of the vessel	0.102 m
Grid	$10 \times 140 \times 15$ and $15 \times 210 \times 15$, for 0.7 m column; $15 \times 260 \times 15$ for 0.85 m column
Flow type	No gas-phase turbulence
Gas–solid model	Eulerian–Eulerian, with kinetic theory
Granular viscosity model	Syamlal and O'Brien (1993)
Drag model	Gibilaro et al. (1985), modified according to Eq. 7
Frictional viscosity model	Schaeffer (1987)
Wall boundary condition for the solid phase	Partial slip
Wall boundary condition for gas phase	No slip
Time step used	0.0001–0.001 s (adaptive)
Max. number of iterations per time step	80
Convergence criteria	MFIX default
Pressure velocity coupling	SIMPLE
Underelaxation factors	0.2 for u, v velocities, granular temperature, granular pressure, and volume fraction, 0.5 for pressure
Maximum solid packing volume fraction	0.6
Discretization scheme	First-order upwind, Superbee
Initial condition	Bed at minimum fluidization
Bed porosity at minimum fluidization	0.4
Bed height at minimum fluidization	0.5 m, 0.61 m
Outlet condition	Atmospheric pressure
Particle–particle restitution coefficient between same phase	0.9
Angle of internal friction	30°
Specularity coefficient	0.005
Gas density	1.21 kg/m^3
Gas viscosity	1.81×10^{-5} kg/m/s

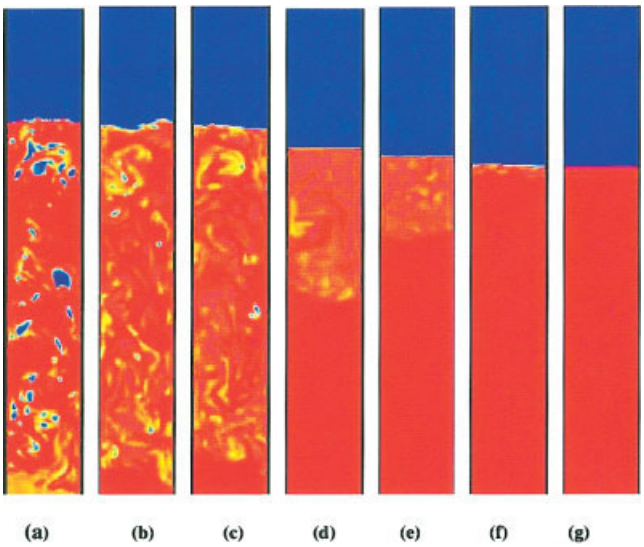

Figure 5. Solid volume fraction contour plots showing the various stages of bed collapse from the moment gas velocity is stopped.

(a) 0 s, (b) 1 s, (c) 1.5 s, (d) 8.5 s, (e) 11.5 s, (f) 14.5 s, (g) 16.5 s. [Color figure can be viewed in the online issue, which is available at www.interscience.wiley.com]

minimum fluidization voidage to reflect the stable homogeneous expansion of an FCC powder.

There are many different techniques available within MFIX for discretizing the governing partial differential equations. For the low-velocity (0.005 m/s) case in which bubbles are not present, the first-order upwind method was used. For the higher-velocity (0.028 m/s) case, the second-order Superbee was used because it gives better resolution of bubbles because of less numerical diffusion compared to that of the first-order methods[30] and is also the preferred method in MFIX for bubbling fluidized beds. All numerical solution parameters (that is, underrelaxation, sweep direction, linear equation solvers, and residual tolerances) were left as their default values in MFIX. Adaptive time stepping was used in all the simulations, which alters the time step depending on the stability and convergence of the solution.

Modeling Procedure and Computation Time

The experimental deaeration test consists of two steps: fluidization of the bed at the chosen superficial gas velocity, followed by deaeration after the air supply is stopped. Our modeling procedure basically reflects the experimental approach. From the initial conditions, fluidizing air was introduced uniformly into the bottom of the bed, which initiated a transient period of bed expansion and increasing voidage. For the lower superficial gas velocity of 0.005 m/s, the model predictions of bed height and voidage were found to be constant after about 60 s of real fluidization time. This was confirmed by carrying on the simulation for another 30 s. After 90 s of fluidization, the inlet gas velocity was set to zero, and deaeration started from that point forward. This was carried on for 30 s until the pressure calculated at various locations in the fluidized bed returned to zero. Thus, the total fluidization–deaeration simulation was carried out for 120 s of real time (5 weeks of computation time on the parallel cluster). For the higher-velocity case (0.028 m/s), the initial transient period lasted for 10 s of real time, followed by 30 s of deaeration. The 40 s of fluidization and deaeration required 6 weeks of computation time, which reflects the smaller time steps and cell size required for a stable solution at the higher velocity.

Results and Discussion

CFD models are able to provide detailed information on the distribution of the gas and solid phases and their velocities inside fluidized beds. Figure 5 presents a series of solid volume fraction contour plots from the time when the fluidizing gas velocity is set to zero. The plots show that bubbles rise rapidly through the bed and disappear about 1 s after the air flow is shut off. There appears to be little sedimentation taking place during this initial period, which is counter to the predictions of Gelderbloom et al.,[13] who reported that sedimentation and bubble escape took place simultaneously. The rapid rise of the bubbles supports the notion that they tend to draw gas out of the bed during deaeration, leading to shorter deaeration times at higher velocities.

Effect of inlet gas velocity

The variation of gauge pressure with time for the inlet gas velocities 0.005 and 0.028 m/s is presented in Figure 6. As the figure shows, the agreement between the experimental data and the CFD model predictions is good for most of the deaeration curve, with the predicted deaeration rate being slightly lower than that found experimentally. For example, for the inlet gas velocity of 0.005 m/s and catalyst mass of 3.17 kg, the predicted time from CFD to reach the first change in slope on the deaeration curve is 10 s, whereas the experimental value is 9 s, which resulted in a predicted deaeration rate of 0.0305 m/s, as opposed to a value of 0.034 m/s obtained from experiments. Figure 6 also compares the predicted deaeration curves at two different gas velocities. Increasing the inlet gas velocity from 0.005 m/s to 0.028 cm/s reduces the deaeration time from 10 to 7 s. Thus the predicted deaeration rate is higher for the higher inlet gas velocity, which is consistent with experimental findings. As noted above, this behavior may be attributable to the rapidly rising bubbles drawing air out of the bed as they escape.

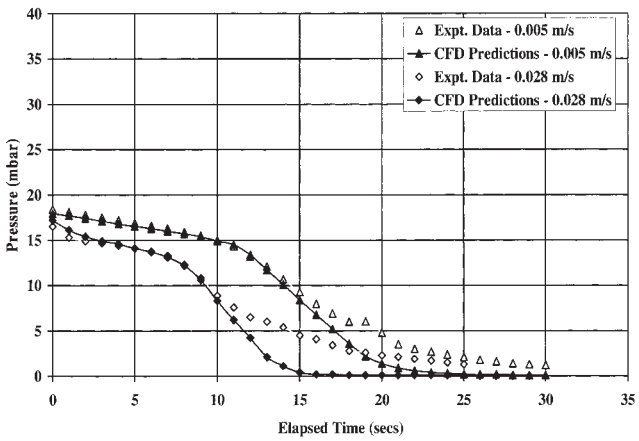

Figure 6. Variation of gauge pressure with time at 0.3048 m above the distributor and catalyst mass 3.17 kg: effect of superficial gas velocity.

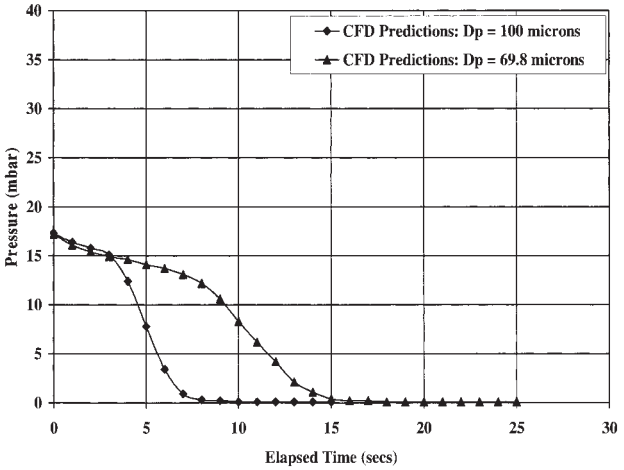

Figure 7. Variation of gauge pressure with time at 0.3048 m above the distributor and catalyst mass of 3.17 kg: effect of particle size.

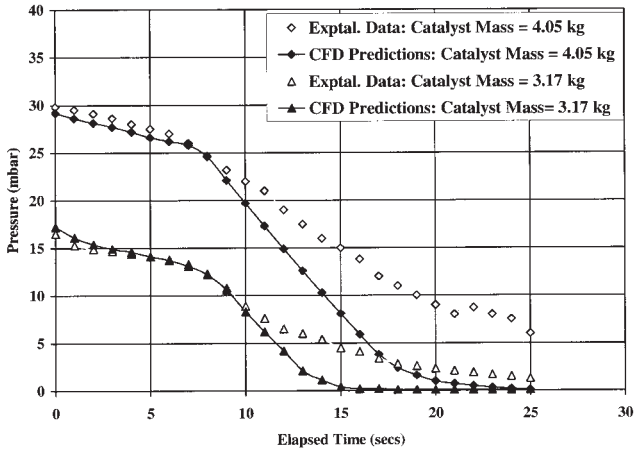

Figure 8. Variation of gauge pressure with time at 0.3048 m above the distributor: effect of catalyst mass.

A significant difference between the experimental data and the CFD predictions is observed after the first change in the slope of the deaeration curve. The change in the slope of the curve is an indication of solid volume fraction more than that at minimum fluidization. Frictional models are applicable once the solid volume fraction in the bed reaches the maximum packing limit, which in most of the cases is taken as equal to that at minimum fluidization. This is done because at such high concentration, frictional interactions between the particles are much more dominant than the collisional interactions. The present frictional models applied for gas–solid fluidization are based on the critical-state theory of soil mechanics, which assumes that during this quasi-static regime, deformation in the solid phase takes place without change in volume.[25,31] The bed thus forms a rigid mass of solid and is nearly incompressible. Although such an assumption simplifies the model, it is applicable for only Geldart B and D particles, which form a packed bed immediately after the minimum fluidization point. However, Geldart A particles, like FCC, retain an appreciable amount of air during deaeration even after the minimum fluidization point is reached and with time would squeeze out this air, thereby deforming the bed with change in volume. This indicates that the present frictional models cannot predict the bed structure below the minimum fluidization point for FCC particles. Thus, a fresh look into these models is necessary.

Effect of mean particle size

Figure 7 illustrates the effect of mean particle size on the deaeration time by comparing the deaeration curves corresponding to mean particle diameters of 100 and 69.8 microns at a gas velocity of 0.028 m/s and a catalyst mass of 3.17 kg. The deaeration time is longer for the larger mean size, indicating that the deaeration rate is faster. Comparison of the CFD predicted deaeration rate of 0.102 m/s with the experimental rate of 0.109 m/s for the particle size of 100 microns once again shows a good agreement (Table 3). The increase in deaeration rate with mean particle size suggests that the simulation is able to capture the experimentally observed role of the fines through a single mean diameter.

Effect of catalyst mass

The deaeration rate for a given FCC catalyst should not be influenced by the mass of catalyst in the test bed—only the value of the pressure above the measurement point should be affected. This is indeed the observed trend in the experimental data as shown in Figure 8 by comparing the deaeration curve for the two different catalyst masses, 3.17 and 4.05 kg. The difference of pressure between the two curves is attributed to the increased weight of the catalyst above the measurement point for the larger bed mass. The CFD model is also capable of capturing the experimental trends. The CFD prediction is also compared with the experimental data for the catalyst mass of 4.05 kg in the same figure and shows good agreement.

Summary of results

The deaeration rate calculated at different heights for all the above cases is summarized in Table 3. The good agreement between the experimental values and the CFD data is evident, with the percentage difference being $<10\%$ in all cases.

Table 3. Comparison of Experimental and Predicted Deaeration Rates

Particle Size (μm)	Catalyst Mass (kg)	Inlet Gas Velocity (m/s)	Height above the Distributor (m)	Deaeration Rate (m/s)		Percentage Difference
				Experimental Data	CFD Prediction	
69.8	3.17	0.005	0.3048	0.034	0.0305	10.3
69.8	3.17	0.028	0.3048	0.0406	0.0417	2.7
100	3.17	0.028	0.3048	0.109	0.102	6.4
69.8	4.05	0.028	0.3048	0.0406	0.0406	0.1

Conclusions

(1) Deaeration time and deaeration rate calculated from the simulations are in very good agreement with the experimental data. The percentage error is $<10\%$ in all cases.

(2) The CFD model properly predicts the relative influence of inlet gas velocity, particle size, and catalyst mass on the deaeration time and deaeration rate.

(3) Good agreement between experimental pressure vs. time data during deaeration and the CFD predictions for two different mean particle sizes shows that the simulations were able to capture the experimentally observed role of fines through a single mean diameter. This raises the possibility that it may not be necessary to implement complicated model equations for multiple particle phases to determine the effect of particle size distribution or the effect of fines on the deaeration rate.

(4) There is considerable difference between the CFD predictions and the experimental data when the bed reaches a nonexpanded state marked by the second change in slope of the deaeration curve. This deviation may arise from the unsuitability for FCC powders of the existing frictional-stress models.

(5) As reported in previous publications from our group, we found that it was necessary to reduce the drag force predicted by the existing drag models to obtain realistic bed expansion when modeling bubbling fluidization. This phenomenon is explained by the interparticle cohesive forces causing agglomeration. The cohesive force may be modeled by assuming it is proportional to the buoyant weight of a particle. This leads to a theoretical basis for the drag correction factor C.

Acknowledgments

The financial support of Total is gratefully acknowledged as is the MFIX-related technical support from the staff of the National Energy Technology Laboratory.

Notation

C = drag equation scale factor
$\bar{\bar{D}}$ = rate of strain tensor, s^{-1}
d_p = mean particle diameter, m
e = particle–particle collision restitution coefficient
$\vec{F}_D$ = gas–solids drag force, N
F_{gs} = gas–solids drag function, kg m^{-3} s^{-1}
$\vec{g}$ = gravitational acceleration vector, m^2/s
g = radial distribution function at contact between same solid phase
H = dense bed height, cm
$\bar{\bar{I}}$ = identity matrix, all components zero except for ones along diagonal
I_{2Dg} = second invariant of the deviator of the strain rate tensor for the gas phase, $1/s^2$
I_{2Ds} = second invariant of the deviator of the strain rate tensor for the solid phase, $1/s^2$
K_1, K_2, K_3, K_4 = parameters in kinetic theory description of solids phase
P = pressure, Pa
P_n = normalized pressure
P_{tot} = total pressure, Pa
Re = particle Reynolds number
$\bar{\bar{S}}_s$ = solid-phase stress tensor, Pa
t = time, s
U = superficial gas velocity, m/s
$\vec{v}$ = velocity vector, m/s

Greek letters

ε = voidage (volume fraction)
ε_g^* = gas voidage at critical packing for switch from viscous to plastic stress
ε_s = volume fraction of the solid phase
ε_s^{cp} = closed packed solids volume fraction
ϕ = internal angle of friction in Eq. 12, degrees
φ = specularity coefficient
λ = second coefficient of viscosity, Pa·s
μ_g = gas viscosity, Pa·s
Θ = granular temperature, m^2/s^2
ρ = density, kg/m^3
$\bar{\bar{\tau}}$ = deviatoric stress tensor, Pa

Subscripts

g = gas phase
mf = minimum fluidization point
pg = of the gas pressure
ps = of the solids pressure
s = solids phase

Superscripts

$*$ = previous value
cp = closed packed
p = plastic regime
tol = tolerance
v = viscous regime

Literature Cited

1. Dry RJ, Shingles T, Judd MR. Two-phase theory and fine powders. *Powder Technol.* 1983;34:213-223.
2. Simone S, Harriott P. Fluidization of fine powders with air in the particulate and the bubbling regions. *Powder Technol.* 1980;26:161-167.
3. Abrahamsen R, Geldart D. Behaviour of gas-fluidized beds of fine powders—Part II. Voidage of the dense phase in bubbling beds. *Powder Technol.* 1980;26:47-55.
4. Bohle W, van Swaaij WPM. Influence of gas adsorption on mass transfer and gas mixing in a fluidized bed. In: Davidson JF, Keairns DL, eds. *Fluidization*. Cambridge, UK: Cambridge Univ. Press; 1978: 167-172.
5. Drinkenburg AAH, Rietema K. Gas transfer from bubbles in a fluidized bed to the dense phase—II: Experiments. *Chem Eng Sci.* 1973; 28:259-273.
6. Formisani B, Girimonte R, Pataro G. The influence of operating temperature on the dense phase properties of bubbling fluidized beds of solids. *Powder Technol.* 2002;125:28-38.
7. Lettieri P, Yates JG, Newton D. The influence of interparticle forces on the fluidization behaviour of some industrial materials at high temperature. *Powder Technol.* 2000;110:117-127.
8. Khoe GK, Ip TL, Grace JR. Rheological and fluidization behaviour of powders of different particle size distribution. *Powder Technol.* 1991; 66:127-141.
9. Geldart D, Wong ACY. Fluidization of powders showing degrees of cohesiveness—II: Experiments on rates of deaeration. *Chem Eng Sci.* 1985;40:653-661.
10. Lorences MJ, Patience GS, Diez FV, Coca J. Fines effects on collapsing fluidized beds. *Powder Technol.* 2003;131:234-240.
11. Peirano E, Delloume V, Leckner B. Two- or three-dimensional simulations of turbulent gas–solid flows applied to fluidization. *Chem Eng Sci.* 2001;56:4787-4799.
12. McKeen TR, Pugsley T. Simulation and experimental validation of a freely bubbling bed of FCC catalyst. *Powder Technol.* 2003;129:139-152.
13. Gelderbloom SJ, Gidaspow D, Lyczkowski RW. CFD simulations of bubbling/collapsing fluidized beds for three Geldart groups. *AIChE J.* 2003;49:854-858.
14. Englehard Corporation. Troubleshooting FCC unit circulation and fluidization problems. The Catalyst Report TI-800. East Windsor, CT: Engelhard Corp. (http://www.refiningonline.com/EngelhardKB/)
15. Grace JR, Sun G. Influence of particle size distribution on the performance of fluidized bed reactors. *Can J Chem Eng.* 1991;69:1126-1134.
16. Yates JG, Newton D. Fine particle effects in a fluidized-bed reactor. *Chem Eng Sci.* 1986;41:801-806.

17. Zenz FA, Othmer DF. Particle and powder physical characteristics. *Fluidization and Fluid Particle Systems*. New York, NY: Reinhold Publishing; 1960:94-135.
18. McKeen TR. *Simulation of the Hydrodynamics of a Fluid Catalytic Cracker Stripper Using Computational Fluid Dynamics*. M.Sc. Thesis. Saskatoon, Saskatchewan, Canada: University of Saskatchewan; 2003.
19. Van Wachem BGM, Schouten JC, van den Bleek CM, Krishna R, Sinclair JL. Comparative analysis of CFD models of dense gas–solid systems. *AIChE J.* 2001;47:1035-1051.
20. Ferschneider G, Mege P. Eulerian simulation of dense phase fluidized beds. *Rev Inst Fr Pet.* 1996;51:301-307.
21. Gibilaro LG, Di Felice R, Waldram SP. Generalised friction factor and drag coefficient correlations for fluid–particle interactions. *Chem Eng Sci.* 1985;40:1817-1823.
22. Ye M. *Multi-Level Modeling of Dense Gas–Solid Two-Phase Flows*. Ph.D. Thesis. Enschede, The Netherlands: University of Twente; 2005.
23. Forsyth AJ, Hutton S, Rhodes MJ. Effect of cohesive interparticle force on the flow characteristics of granular material. *Powder Technol.* 2002;126:150-154.
24. Rhodes MJ, Wang XS, Nguyen M, Stewart P, Liffman K. Use of discrete element method simulation in studying fluidization characteristics: Influence of interparticle force. *Chem Eng Sci.* 2001;56:69-76.
25. Schaeffer DG. Instability in the evolution equations describing incompressible granular flow. *J Diff Eq*. 1987;66:19-50.
26. Lun CKK, Savage SB, Jeffrey DJ, Chepurniy N. Kinetic theories for granular flow: Inelastic particles in Couette flow and slightly inelastic particles in a general flow field. *J Fluid Mech.* 1984;140:223-256.
27. Syamlal M, O'Brien TJ. Computer simulation of bubbles in a fluidized bed. *AIChE Symp Ser.* 1989;85:22-31.
28. Johnson PC, Jackson R. Frictional–collisional constitutive relations for granular materials, with application to plane shearing. *J Fluid Mech.* 1987;176:67-93.
29. Benyahia S, Arastoopour H, Knowlton TM, Massah T. Simulation of particles and gas flow behavior in the riser section of a circulating fluidized bed using the kinetic theory approach for the particulate phase. *Powder Technol.* 2000;112:24-33.
30. Guenther C, Syamlal M. The effect of numerical diffusion on isolated bubbles in a gas–solid fluidized bed. *Powder Technol.* 2001;116:142-154.
31. Srivastava A, Sundaresan S. Analysis of a frictional–kinetic model for gas-particle flow. *Powder Technol.* 2003;129:72-85.
32. Molerus O. Interpretation of Geldart's Type A, B, C and D powders by taking into account interparticle cohesion forces. *Powder Technol.* 1982;33:81-87.
33. Rietema K. *The Dynamics of Fine Powders.* Essex, UK: Elsevier Science Publishers; 1991.

Appendix

For cohesive particles, the force balance for a single particle in a gas–solid fluidized bed may be written as

$$F_{Dc} = F_B + F_C \tag{A1}$$

where F_{Dc} is the drag force on a single particle in a fluidized bed, F_B is the buoyant weight on a single particle in a fluidized bed, and F_C is the cohesive force on a single particle arising from particle–particle interactions.

The cohesive force F_C in a fluidized bed has been suggested to be proportional to the buoyant weight of a particle and can be expressed as[32]

$$F_C = K\,\frac{\pi d_p^3 \varepsilon(\rho_p - \rho_f)\,g}{6} \tag{A2}$$

where K is the proportionality constant and is a measure of the cohesiveness of particles. Thus for noncohesive particles $K = 0$ and for cohesive particles $K > 1$.

Expanding Eq. A1 in terms of the fundamental parameters we obtain

$$C_{Dc}\,\frac{\rho u^2 \pi d_p^2}{8} = \frac{\pi d_p^3 \varepsilon(\rho_p - \rho_f)\,g}{6} + K\,\frac{\pi d_p^3 \varepsilon(\rho_p - \rho_f)\,g}{6} \tag{A3}$$

where C_{Dc} is the drag coefficient for a cohesive particle.

Rearranging Eq. A3 we obtain the drag coefficient for cohesive particles as

$$C_{Dc} = \frac{4}{3}\,(1 + K)\,\frac{\varepsilon d_p}{u^2}\left(\frac{\rho_p - \rho}{\rho}\right)g \tag{A4}$$

For noncohesive particles, with $K = 0$, the expression for the drag coefficient becomes

$$C_D = \frac{4}{3}\,\frac{\varepsilon d_p}{u^2}\left(\frac{\rho_p - \rho}{\rho}\right)g \tag{A5}$$

By comparing Eqs. A4 and A5 we see that the relationship between the drag coefficient for cohesive and noncohesive particles is

$$C_{Dc} = (1 + K)C_D \tag{A6}$$

Following the approach of Gibilaro et al.,[21] the relationship between the cohesive drag coefficient and the drag coefficient under terminal conditions can be written as

$$C_{Dc} = C_{Dt}\varepsilon^{1-2n} \tag{A7}$$

By combining Eqs. A6 and A7 the noncohesive particle drag coefficient can be written as

$$C_D = \frac{1}{(1 + K)}\,C_{Dt}\varepsilon^{1-2n} \tag{A8}$$

All of the gas–solid drag models published in the literature are based on a noncohesive drag coefficient, which must be reduced by a factor of $1/(1 + K)$ for cohesive particles.

The value of the parameter K can be determined from theory. The cohesive force for the FCC catalyst (mean diameter 70 microns), reported by Rietema,[33] is approximately 1×10^{-3} g cm^{-2} s^{-1} and the buoyant weight on a single catalyst particle is 3.38×10^{-4} g cm^{-2} s^{-1}. Thus, the ratio of the two forces, that is, K in Eq. A2, is 2.95. Using this value in Eq. A8 gives a factor of $C = 0.25$ by which the drag coefficient for a noncohesive particle has to be reduced to include the effect of the cohesive force on the drag coefficient.

Manuscript received Sept. 26, 2005, and revision received Jan. 26, 2006.